

# EFFECTS OF A Cu ADDITION ON THE CORROSION RESISTANCE OF LOW-ALLOY PRE-HARDENED PLASTIC MOLD STEEL

## VPLIV DODATKA BAKRA NA KOROZIJSKO ODPORNOST MALOLEGIRANEGA ORODNEGA JEKLA ZA BRIZGANJE PLASTIKE

Xuan Chen, Jiayuan Li, Zhi Li, Junwan Li, Xiaochun Wu\*

School of Materials Science and Engineering, Shanghai University, Shanghai 200444, China

Prejem rokopisa – received: 2022-04-04; sprejem za objavo – accepted for publication: 2022-06-09

doi:10.17222/mit.2022.465

The influence of Cu on the corrosion performance of low-alloy Cu-bearing pre-hardened plastic mold steel was investigated and compared with non-Cu-bearing mold steel using transmission electron microscopy (TEM), scanning electron microscopy (SEM), X-ray diffraction (XRD), salt-spray tests and electrochemical impedance spectroscopy (EIS). The results reveal that the formed rust layer is composed of  $\alpha$ -FeOOH,  $\beta$ -FeOOH,  $\gamma$ -FeOOH,  $\text{Fe}_3\text{O}_4$  and large amounts of amorphous compounds. The corrosion product in the early stages of corrosion is loose and porous but becomes denser and more tightly bound to the steel matrix in the later stages, and the corrosion rate of Cu-bearing steel decreases with the increasing corrosion time. With a further Cu addition, the free-corrosion potential of Cu-bearing steel increases and, consequently, the electrochemical impedance, the capacitive single semicircular arc on the impedance spectra and the charge transfer resistance are also significantly enhanced. Therefore, Cu effectively enhances the corrosion resistance of pre-hardened mold steel, prolonging its service life and ensuring a high quality and shape fidelity of molded plastic products.

Keywords: copper, plastic mold steel, corrosion resistance, electrochemical analysis, salt spray test

Avtorji opisujejo vpliv dodatka bakra na korozijske lastnosti toplotno obdelanega malolegiranelega orodnega jekla za oblikovanje plastike. Primerjajo jih s podobnim nelegiranim jeklom (brez dodatka bakra). Za karakterizacijo preiskovanih materialov so uporabili presežno in vrstično elektronsko mikroskopijo (TEM in SEM), rentgensko difrakcijo (XRD), test z razprševanjem slanice in elektrokemijsko impedančno spektroskopijo (EIS). Rezultati analiz so pokazali nastanek korozijske plasti na površini jekla, ki je bila sestavljena iz  $\alpha$ -FeOOH,  $\beta$ -FeOOH,  $\gamma$ -FeOOH,  $\text{Fe}_3\text{O}_4$  in velike količine amorfnih spojin. V začetni fazi korozije je bil korozijski produkt porozen in puhel. V kasnejših fazah je postal gostejši, bolj tesno povezan s kovinsko osnovo jekla in hitrost korozije z bakrom legiranega jekla se je s časom trajanja korozije zmanjševala. Dodatek bakra je povečal prosti korozijski potencial jekla in posledično so se tudi izboljšale elektrokemijska impedanca, enojni kapacitivni polkrožni oblok na impedančnem spektru in upornost prenosa naboja. Na osnovi izvedene raziskave so ugotovili, da legiranje poboljšanelega orodnega jekla z bakrom učinkovito izboljša njegovo korozijsko odpornost in podaljša njegovo dobo trajanja oz. življenjsko dobo orodja, kar posledično tudi zagotavlja visoko kakovost in natančnost oblikovanja izdelkov iz plastike.

Ključne besede: baker, orodno jeklo za brizganje plastike, korozijska odpornost, elektrokemijska analiza, test z razprševanjem slanice

## 1 INTRODUCTION

Molds composed of pre-hardened steel are critical components in the manufacture of a wide range of products, and increasing the tool life of pre-hardened mold steel to improve production efficiency, reduce costs and maintain the quality of molded products remains a great challenge.<sup>1,2</sup> Pre-hardened mold steels, such as those belonging to the medium-carbon low-alloy steel family AISI P20 and its derivatives DIN 1.2738 (German grade) and 718 (Swedish grade), have been widely used in industry.<sup>3,4</sup> The lifespan of plastic mold steel is determined by material deterioration such as wear, cracking and corrosion, with corrosion being the main factor.<sup>5-7</sup> Therefore, corrosion management is critical. Corrosion performance is governed mainly by the environment and the

material properties, and corrosion resistance can be improved by alloying. For instance, Cr and Cu are well-known alloying elements<sup>8,9</sup> that protect steel against corrosion induced by weather and acid exposure, respectively.

Most studies on the corrosion behavior of low-alloy steels focused on corrosion in a single medium, either the atmosphere or an aqueous solution. It has been suggested that a dense rust layer composed of aggregated fine rust particles serves as a good barrier against mass transfer and that alloying elements can contribute to the formation of fine particle rusts. Cu inhibits the crystallization and growth of rust particles, whereas Cr enhances the formation of uniform amorphous ferric oxyhydroxide, thus promoting the development of a compact rust layer.<sup>10</sup> Moreover, Cu can reduce the conductivity of the rust layer, thus decreasing the rate of electrochemical iron dissolution.<sup>11</sup> Choi et al.<sup>12</sup> revealed that Cr and Cu

\*Corresponding author's e-mail:  
wuxiaochun@shu.edu.cn (Xiaochun Wu)

compounds promote the formation of a protective rust layer on steel in aqueous conditions as they do under atmospheric conditions. However, a Cu addition to plastic mold steel and its effect on the corrosion resistance have not been widely studied.

This study clarifies the influence of added Cu as an acid-resistant element on the corrosion of low-alloy pre-hardened plastic mold steel. Pre-hardened plastic mold steels, with and without Cu, were characterized by scanning electron microscopy (SEM), high-resolution transmission electron microscopy (HRTEM), X-ray diffraction (XRD), electrochemical impedance spectroscopy (EIS) and accelerated corrosion via salt-spray tests; the results were analyzed and compared to determine the mechanism for corrosion resistance enhancement by Cu.

## 2 EXPERIMENTAL PART

### 2.1 Materials

The chemical compositions of SDP1 and SDP1Cu steel are listed in **Table 1**. Steel samples of (15 × 15 × 40) mm in size were cut from a round rod and heated at 950 °C for 2 h so that copper could be solid dissolved into the steel matrix. A bainite structure was obtained with slow cooling at 0.1 °C/s followed by tempering at 500 °C for 2 h.

**Table 1:** Chemical compositions (w/%) of SDP1 and SDP1Cu steels

Material	C	Si	Mn	Cr	Ni	Mo	Cu	Al	Fe
SDP1Cu	0.20	0.60	1.55	1.12	0.60	0.22	1.16	0.11	Bal
SDP1	0.21	0.65	1.60	1.08	0.50	0.20	–	–	Bal

### 2.2 Corrosion test

EIS measurements were carried out using a standard electrochemical workstation (Gamry Reference 600) with a three-electrode cell containing a saturated calomel electrode (SCE) as the reference electrode, a platinum foil as the counter electrode and the SDP1 and SDP1Cu steel samples as the working electrodes. All the experiments were performed in a 0.5 w/% NaCl solution, which was prepared by dissolving analytically pure NaCl in deionized water at room temperature ((25 ± 2) °C). In addition, before EIS and potentiodynamic polarization measurements, the open-circuit potential (OCP) of each sample was measured for 45 min until a stable potential was reached. The EIS tests were performed with an amplitude perturbation of ± 10 mV and a frequency range of 10<sup>5</sup> Hz to 10<sup>-2</sup> Hz over the OCP. The potentiodynamic polarization measurements were conducted at a scanning rate of 0.5 mV/s (30 mV/min), from -100 mV below the OCP to 300 mV with respect to the SCE. In order to get reliable results, at least three specimens of each alloy with different nitrogen contents were used, and the results were fitted and analyzed using the measurement instrument software.

Corrosion properties were studied through salt-spray tests. SDP1 and SDP1Cu steel were cut into (15 × 15 × 2) mm test samples. The salt-spray test was performed according to Chinese standard GB/T 10125-2012 in an artificial atmosphere with the following conditions: the NaCl concentration of the sprayed solution was 50 g/L (5.0 % NaCl), the temperature was 35 °C, the pH range of the solution was 6.5–7.2 and the samples were placed in a testing chamber with the unprotected side facing upwards at an angle of 15° from the vertical. The salt-spray experiments were conducted for (48, 96 and 192) h.

### 2.3 Microstructure observation

The microstructures of the samples were observed using an optical microscope, a Carl Zeiss SUPRA 40 field emission SEM, and a JEM-2100F TEM. For SEM observation, the samples were mechanically ground with sandpaper, polished, and then etched in a 4 % nital solution. For TEM observation, 500-μm thick discs were first mechanically thinned to approximately 50-μm thick foils and then electropolished by a twin-jet electro polisher in a solution of 10 % volume fraction of perchloric acid and 90 % volume fraction of ethanol. After the salt-spray test, an 18 kW D/MAX X-ray diffractometer (Japan Rigaku Corporation) was used to continuously scan the samples with a Cu-Kα ray. The XRD acceleration voltage was 40 kV, the scanning speed was 4 °/min, and the scanning-angle range was 20°–70°.

### 2.4 Direct mass-loss measurements

Prior to the salt-spray exposure, the specimens for mass-loss measurements were rinsed with acetone, air-dried and weighed using a microbalance. After each exposure, the specimens were descaled via immersion in a solution of 500 mL HCl + 3.5 g hexamethylenetetramine and then successively rinsed in distilled water and acetone. The specimens were then air-dried and re-weighed in order to calculate the mass loss resulting from corrosion. The mass-loss rate,  $V_s$ , of the material was calculated according to Equation (1):

$$V_s = \frac{m_0 - m_1}{S \cdot t} \quad (1)$$

where  $m_0$  is the mass in g before the test,  $m_1$  is the mass in g after the test,  $S$  is the surface area of the specimen in m<sup>2</sup> and  $t$  is the corrosion test duration in h.

## 3 RESULTS

### 3.1 Microstructure

**Figures 1a** and **1b** show SEM morphologies of the SDP1Cu and SDP1 steel microstructures. The SEM morphologies show the typical lath bainite and the classic granular bainite. Each lath bainite grain is composed of several lath bundles with different orientations. Some granular islands of the secondary phase are distributed in

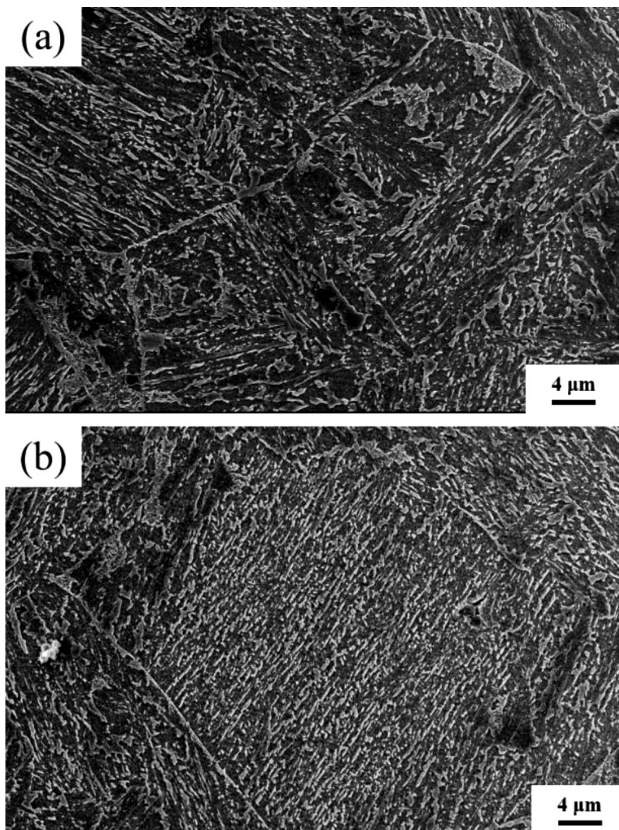


**Figure 1:** SEM scanning images after heat treatment: a) SDP1Cu steel, b) SDP1 steel

the equiaxed bainitic ferrite matrix. The sizes of the islands are unequal, and most of them are in the 1–10  $\mu\text{m}$  range. Several previous studies identified the islands as martensite-austenite (M-A) constituents.<sup>13</sup> There are M-A islands both inside the grains and at the grain boundaries. The M-A islands at the grain boundaries decompose preferentially, and adjacent decomposed structures are connected. Precipitated interfaces nucleate and grow preferentially at the grain boundaries, enriching the grain boundaries.<sup>14</sup>

**Figure 2** shows a bright field image, a dark field image and diffraction pattern of SDP1Cu steel. A continuous arrangement of rod-like carbide is observed. The carbide was determined to be  $\text{M}_{23}\text{C}_6$ -type carbide based on the diffraction pattern of the crystal axis band [112]. As the copper-rich precipitated phase was very fine, an HRTEM analysis of the SDP1Cu steel samples was performed. As can be seen from **Figure 3**, the precipitated phase is composed of short rods of 10–20 nm in length. This is the copper-rich precipitated phase. The diffraction pattern after Fourier transform confirms a face-centered cubic structure, with a maximum length of the long axis of about 20 nm.

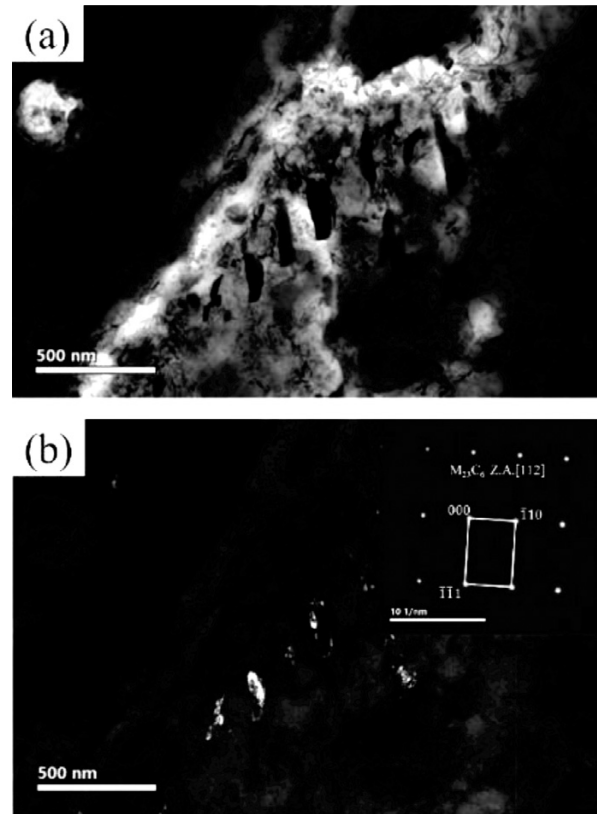


**Figure 2:** TEM image of SDP1Cu steel: a) bright field image, b) dark field image and diffraction pattern

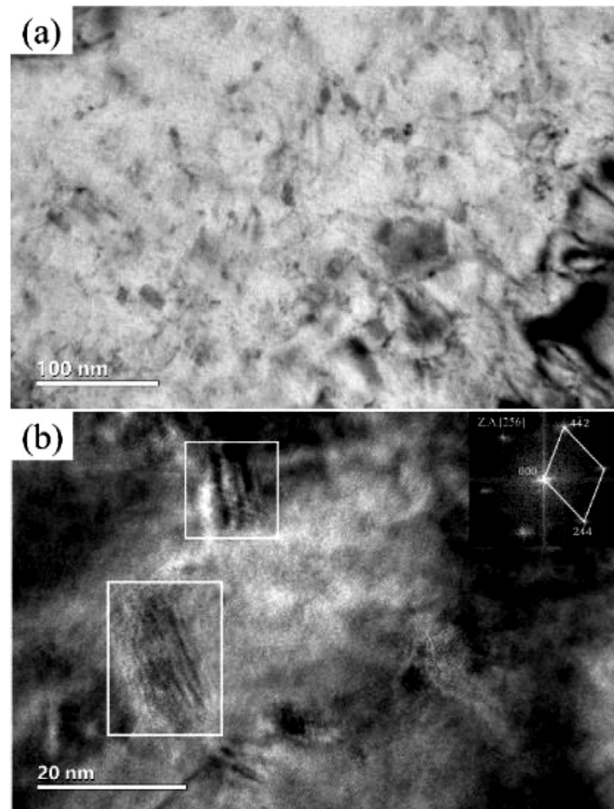


**Figure 3:** HRTEM of SDP1Cu steel: a) microstructure, b) diffraction pattern of rod-like structures

### 3.2 Electrochemical measurements

Figure 4a shows the open-circuit potential versus time curves of the steels tested in a 0.5 % NaCl solution. Generally, the smaller the absolute value of the open-circuit potential after stabilization, the smaller is the self-corrosion potential of the material in the current corrosion environment, indicating better corrosion resistance. The two types of steel showed the same behavior,

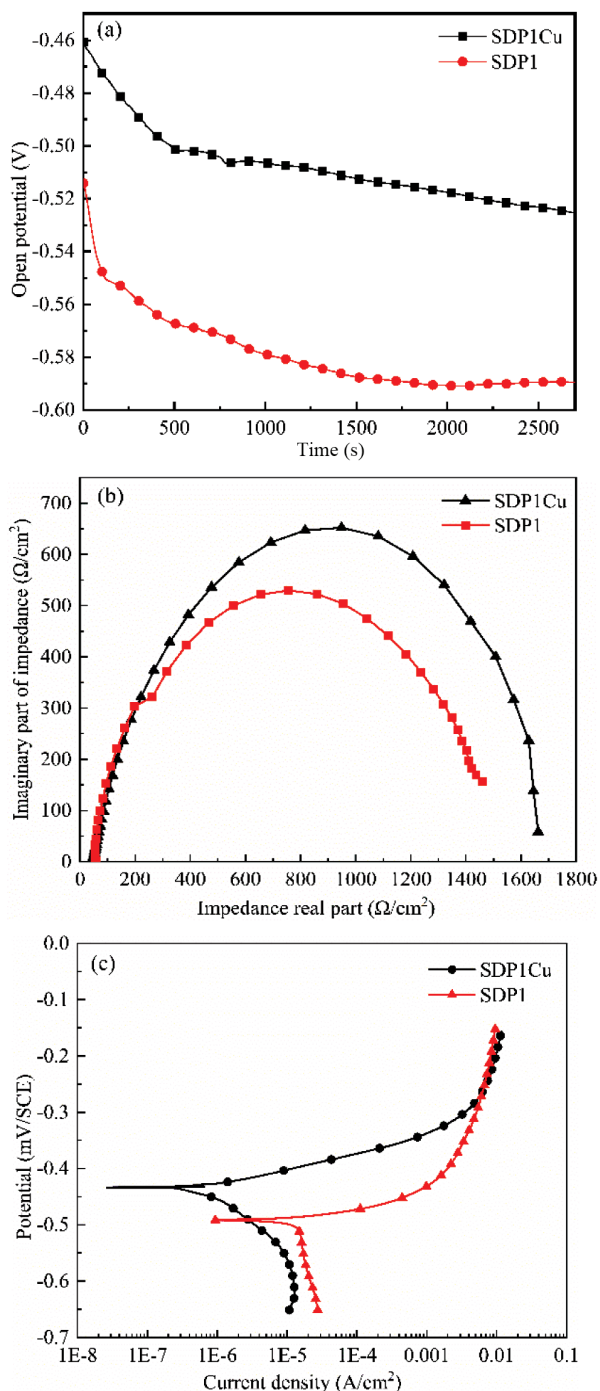


Figure 4: Electrochemical experiment results: a) open-circuit potential curves, b) Nyquist impedance diagrams, c) potential polarization curves

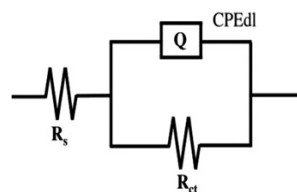


Figure 5: Equivalent circuit adopted to fit the EIS data

that is, a negative shift of the open-circuit potential in the initial stage is followed by a gradual stabilization. Therefore, both SDP1Cu and SDP1 exhibited activation behavior in the 0.5 % NaCl aqueous environment.

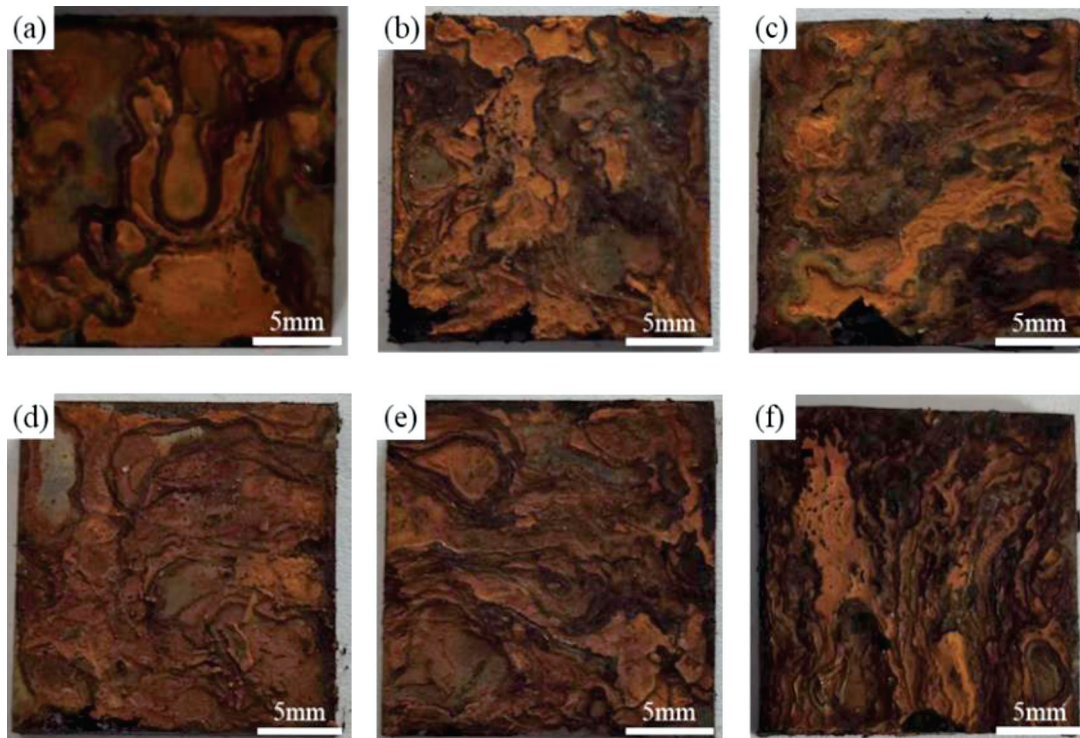
Figure 4b shows Nyquist plots of the electrochemical impedance of the two experimental steels. The capacitive reactance arc indicates the resistance to electrochemical reactions at the metal interface and the double-layer capacitance of the material cross-section, while the size of the arc reflects the charge transfer resistance. The electrochemical-impedance spectra of the two experimental steels exhibit single capacitance-arc characteristics, indicating that the addition of Cu does not change the main characteristics of the impedance spectra. An equivalent circuit diagram can be obtained through fitting, as shown in Figure 5. The Nyquist diagram shows that the arc resistance diameter of the Cu-containing experimental steel increases significantly, indicating that it is more difficult to transfer charge at the electrode solid-liquid interface during the corrosion process, decreasing the corrosion rate. The corrosion resistance of SDP1Cu is higher than that of SDP1, confirming that the addition of Cu enhances corrosion resistance.

Figure 4c shows the polarization curves of the tested steels. It can be observed that the cathodic polarization curves of the two steels have similar shapes, but the corrosion potential is shifted positively after adding Cu. The moving point polarization curve of the Cu-containing steel moves upward as a whole, and the electrode potential increases. This is because the layer of corrosion products covers the surface of the matrix, meaning that Cu ions are enriched on the surface of the sample, increasing the potential. When the corrosion current density is the same, the more positive the corrosion potential, the better is the corrosion resistance of the material. The increase in the corrosion potential indicates that the standard voltage difference between the cathode and anode of the electrochemical reaction decreases without polarization, so Cu has a tendency to thermodynamically reduce electrochemical corrosion.

The Tafel extrapolation method was used to fit the electrochemical data, and the corrosion rate was calculated using the self-corrosion current density according to Equation (2):

$$CR = 3.6 \times 10^7 \times \frac{iM}{zF} \quad (2)$$

where CR is the corrosion rate in g/(m<sup>2</sup>·h), i is the self-corrosion current density in A/cm<sup>2</sup> obtained from



**Figure 6:** Macroscopic morphology after accelerated corrosion in the salt-spray environment: a) SDP1Cu – 48 h, b) SDP1Cu – 96 h, c) SDP1Cu – 192 h, d) SDP1 – 48 h, e) SDP1 – 96 h, f) SDP1 – 192 h

the polarization curve,  $M$  is the molar mass of iron in g/mol,  $z$  is the chemical valence of the material, and  $F$  is Faraday's constant in C/mol. The results are summarized in **Table 2**. The SDP1Cu steel shows the highest electrode potential and the best surface film stability owing to the addition of Cu and Ni, which increase the electrode potential.<sup>15</sup>

**Table 2:** Fitting data for the potential polarization curve

Material	$E_{corr}$ (V/SCE)	$I_{corr}$ ( $\times 10^{-4}$ (A/cm <sup>2</sup> ))	$CR$ (g/(m <sup>2</sup> ·h))
SDP1Cu	-0.433	0.124	0.086
SDP1	-0.491	1.458	1.012

### 3.3 Salt spray test

**Figure 6** shows the surface micromorphology of SDP1Cu and SDP1 steels after corrosion for different durations in a salt-spray environment. As can be observed, there are still small areas not covered by the rust layer after 48 h of accelerated corrosion. When the corrosion duration was increased to 192 h, the rust layer completely covered the surface of the sample. The formed rust has two layers. The outer rust layer is yellowish brown, brittle in texture and easily falls off from the sample surface. The inner rust layer is black, tightly combined with the matrix and not easily dislodged.

**Figure 7** shows the corrosion-rate statistics for SDP1Cu and SDP1 steel. When the salt-spray test duration is (48, 96 and 192) h, the corrosion rate of SDP1Cu

steel is (1.60, 1.19, and 0.987) g/(m<sup>2</sup>·h), respectively, while the corrosion rate of SDP1 steel is (1.58, 1.35, and 1.21) g/(m<sup>2</sup>·h), respectively. With the increase in the corrosion time, the corrosion rates of both types of steel gradually decrease, indicating that the rust layer is hindering the elemental diffusion process between the matrix and the external corrosion solution, thus reducing the corrosion rate of the materials. At the same time, during salt-spray accelerated corrosion, the corrosion rates of the two steels are similar at the initial stage of corrosion, indicating that although Cu can improve the electrode potential of the matrix, it does not effectively reduce the initial corrosion rate in a harsh environment. The corrosion rate of SDP1Cu steel decreases much faster than

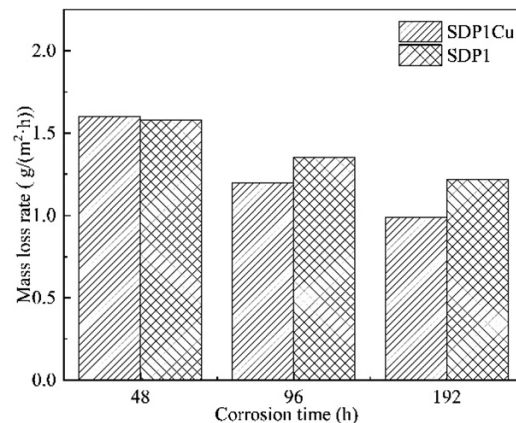


**Figure 7:** Corrosion-rate statistics

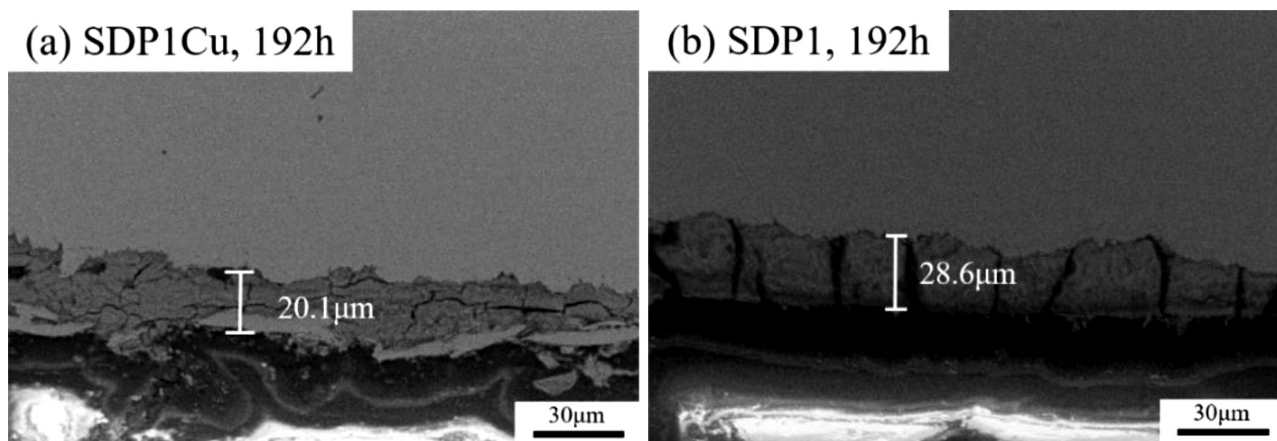


Figure 8: SEM images of the rust layer cross-sections: a) SDP1Cu, b) SDP1

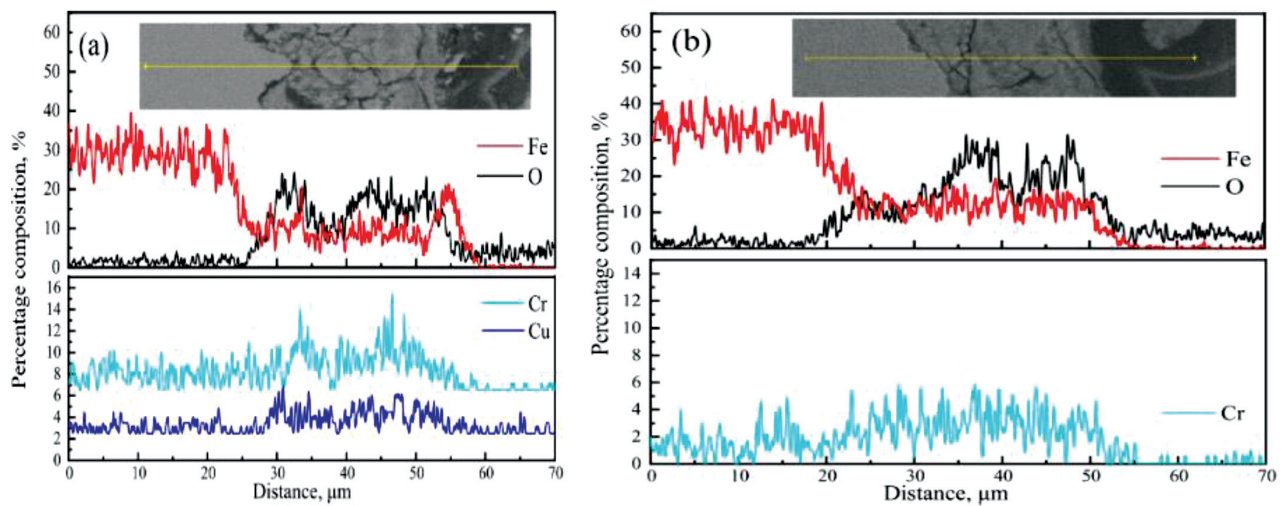


Figure 9: Line-scan composition analysis of the rust layer formed after salt-spray tests: a) SDP1Cu, b) SDP1

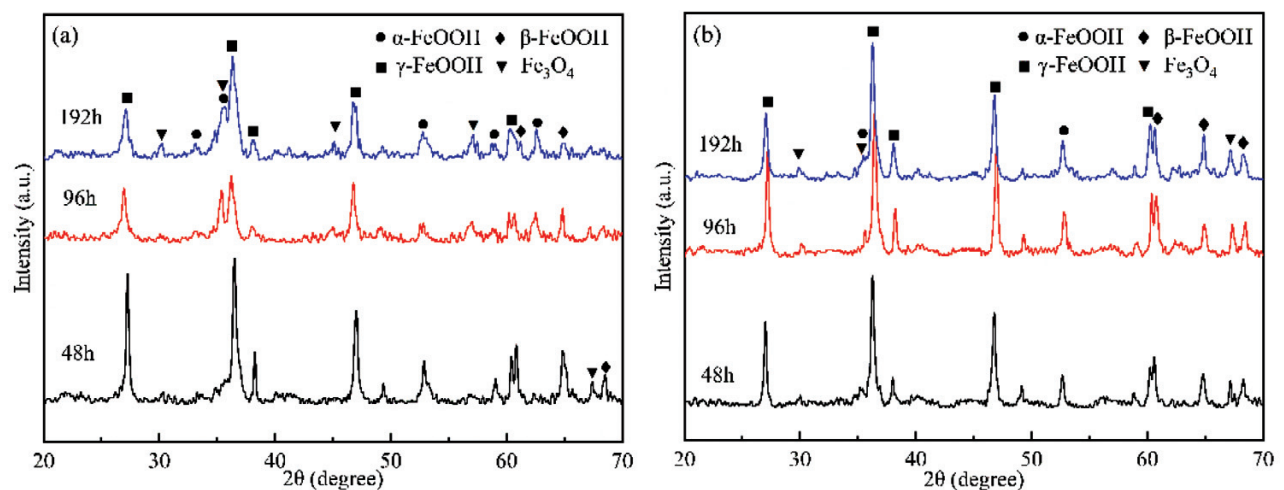


Figure 10: Changes in the rust-layer composition and relative content of each product with the salt-spray time: a) SDP1Cu steel, b) SDP1 steel

that of SDP1 steel. This indicates that in the salt-spray corrosion environment, Cu has no obvious effect in the early stage, but can effectively improve the density and integrity of the rust layer after the rust layer is produced so as to effectively reduce the corrosion rate.

Samples were selected for cold mounting and the rust layer was observed. SEM images of the experimental steels after the salt-spray test for 192 h are shown in **Figure 8**. The thickness of the rust layer of the Cu-containing steel sample is about 20  $\mu\text{m}$ , which is significantly lower than that of the non-Cu-containing steel sample (about 28  $\mu\text{m}$ ).

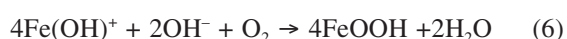
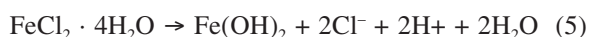
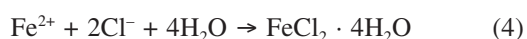
**Figure 9** shows energy dispersive X-ray analysis results of the SDP1 and SDP1Cu rust layers. Cr enriched the rust layer of both steels as it can promote the formation of a protective rust layer and reduce the anodic dissolution of the matrix alloy. Meanwhile, Cu enriched the rust layer of SDP1Cu, indicating that Cu promotes the densification and completion of the rust-layer structure. Other researchers have also found that Cu enrichment of other alloy steels can promote the densification of the rust layer, prevent oxygen diffusion to the surface of the matrix and reduce the electrical conductivity of the rust-layer surface so as to protect the material and reduce its corrosion.

**Figure 10** shows the variation in the surface rust-layer composition and the relative content of each phase in SDP1Cu and SDP1 steel for different salt-spray test durations. After the salt-spray test, the compositions of the rust layers on the surfaces of the two steel samples are similar. The rust layers are mainly composed of  $\alpha$ -FeOOH,  $\beta$ -FeOOH,  $\gamma$ -FeOOH,  $\text{Fe}_3\text{O}_4$  and large amounts of amorphous compounds. These amorphous compounds are mainly microcrystalline oxides or hydroxides and could not be identified by XRD.<sup>16</sup>  $\alpha$ -FeOOH is more continuous and compact; it is non-conductive, effectively protecting the matrix.

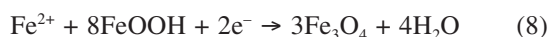
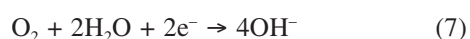
#### 4 DISCUSSION

The corrosion of plastic mold steel in an aqueous environment is dominated by electrochemical corrosion. In etchant solutions containing dissolved oxygen, the following anodic and cathodic reactions occur.<sup>8,17</sup>

Anodic reactions are presented in Equations (3) to (6):



Cathodic reactions are presented in Equations (7) and (8):



Corrosion products of low-alloy steel generally consist of  $\alpha$ -FeOOH,  $\beta$ -FeOOH,  $\gamma$ -FeOOH,  $\text{Fe}_3\text{O}_4$  and amorphous products. During long-term corrosion of steel,  $\gamma$ -FeOOH is first formed on the surface of the matrix. Then, it develops into amorphous FeOOH, which is eventually transformed into stable  $\alpha$ -FeOOH.  $\alpha$ -FeOOH exhibits good continuity and density, and does not conduct electricity, effectively protecting the matrix. An addition of alloying elements can enrich the rust-layer cracks and prevent the corrosive medium from contacting the matrix, thus reducing the corrosion rate<sup>18</sup>. According to a previous study,<sup>19</sup> an addition of Cu promotes the transformation of  $\gamma$ -FeOOH into the most stable corrosion phase,  $\alpha$ -FeOOH, thus reducing the electrical conductivity of the corroding rust layer and slowing down the electrochemical corrosion rate.

The rust layer on the surface of low-alloy steel is divided into two sublayers: the outer rust layer, which is loose and porous exhibiting poor protection, and the inner rust layer, which is mainly composed of dense  $\alpha$ -FeOOH and firmly bonded to the matrix. The corrosion products of the experimental steel without Cu are thick and loose, with many cracks, and the interface between the corrosion products and the matrix is uneven with a few corrosion pits. In contrast, the corrosion products of the experimental steel with Cu are thin and compact, and the interface with the matrix is smooth.

From surface analyses obtained with different techniques, it was confirmed that a film containing elemental Cu was formed on the SDP1Cu steel surface after a corrosion test. Hao et al.<sup>20</sup> reported that elemental Cu is concentrated on the surface of Cu-containing carbon steel immersed in a strongly acidic NaCl aqueous solution, and the results of the present study are in good agreement with this previous report. The mechanism for the improvement of corrosion resistance of steel due to the formation of elemental Cu on a steel surface in a strongly acidic environment was examined in detail by Hoog et al.<sup>9</sup> based on electrochemical measurement results. A Cu-enriched layer is formed on the steel surface due to base metal dissolution and the re-deposition of Cu with lower solubility. Ishii et al.<sup>21</sup> suggested that Cu improves the corrosion resistance of steel surfaces and inhibits anodic reactions. Due to the Cu and Cr enrichment, the corrosion rust layer on low-alloy steel generates a complex iron chromium copper oxide, refines the rust layer of particles and fills micro cracks and holes of the rust layer, thereby increasing the rust-layer density, blocking the channels of direct contact with the corrosive medium and the matrix and improving the corrosion resistance. Cu exists in the rust layer formed in various compound salts, being the core of FeOOH crystallization. Due to the milling and densification, the inner rust layer reduces the ion channels and anode area; it also reduces the formation of  $\text{Fe}_3\text{O}_4$ , the conductivity and the corrosion rate.

## 5 CONCLUSIONS

The addition of Cu to low-alloy plastic mold steel significantly improves the corrosion resistance of the material. The following conclusions can be drawn from this study:

1) Cu and other elements can improve the self-corrosion potential of SDP1Cu steel and reduce the corrosion rate and self-corrosion current density of the material.

2) During the salt-spray test, the corrosion rate of SDP1Cu steel decreased from 1.60 g/(m<sup>2</sup>·h) to 0.988 g/(m<sup>2</sup>·h) and that of SDP1 steel decreased from 1.579 g/(m<sup>2</sup>·h) to 1.21 g/(m<sup>2</sup>·h) with the increase in the salt-spray duration due to the generation of a rust layer on the surface of the material. The protective effect of the formed corrosion layer is enhanced in SDP1Cu steel.

3) An elemental Cu-enriched layer was formed on the corroded surface of Cu-containing steel. Polarization curves confirm that this Cu-enriched layer suppresses both anodic and cathodic reactions.

4) The corrosion products of the two steels are mainly composed of  $\alpha$ -FeOOH,  $\beta$ -FeOOH,  $\gamma$ -FeOOH, and Fe<sub>3</sub>O<sub>4</sub>.  $\gamma$ -FeOOH is formed in the early stage and gradually transforms to  $\alpha$ -FeOOH with the increase in the corrosion time.

The new steel, SDP1Cu, can improve the corrosion resistance of plastic molds and prolong their service lives.

## Acknowledgements

This work was supported by the National Key R&D Program of China (Grant Nos. 2016YFB0300400 and 2016YFB0300404).

## 6 REFERENCES

- R. Wu, J. Li, W. Li, X. Wu, X. Jin, S. Zhou, L. Wang, Effect of metastable austenite on fracture resistance of quenched and partitioned (Q&P) sheet steels, *Mat. Sci. Eng. A*, 657 (2016), 57–63, doi:10.1016/j.msea.2016.01.051
- H. Hoseiny, F. G. Caballero, R. M'Saoubi, B. Högman, J. Weidow, H. O. Andrén, The influence of heat treatment on the microstructure and machinability of a prehardened mold steel, *Metall. Mater. Trans. A*, 46 (2015) 5, 2157–2171, doi:10.1007/s11661-015-2789-4
- H. Liu, P. Fu, H. Liu, C. Sun, N. Du, D. Li, Limitations of the homogenization process of bulk martensitic mold steel depending on the comprehensive manifestation of various strengthening, *J. Mater. Sci. Technol.*, 117 (2022), 120–132, doi:10.1016/j.jmst.2021.10.046
- F. Beaudet, C. Blais, H. Lehuy, B. Voyzelle, G. L'espérance, J.-P. Masse, M. Krishnadev, Improvement of hardenability and static mechanical properties of P20+ 0.5 Ni mold steel through additions of vanadium and boron, *ISIJ Int.*, 52 (2012) 3, 424–433, doi:10.2355/isijinternational.52.424
- H. Hoseiny, F. G. Caballero, B. Hogman, D. San Martin, C. Capdevila, L. G. Nordh, H. O. Andren, The effect of the martensitic packet size on the machinability of modified AISI P20 prehardened mold steel, *J. Mat. S.*, 47 (2012) 8, 3613–3620, doi:10.1007/s10853-011-6208-y
- F. J. G. Silva, R. P. Martinho, R. J. D. Alexandre, A. P. M. Baptista, Increasing the wear resistance of molds for injection of glass fiber reinforced plastics, *Wear*, 271 (2011) 9–10, 2494–2499, doi:10.1016/j.wear.2011.01.074
- E. Boztepe, A. C. Alves, E. Ariza, L. A. Rocha, N. Cansever, F. Toptan, A comparative investigation of the corrosion and tribo-corrosion behaviour of nitrocarburized, gas nitrided, fluidized-bed nitrided, and plasma nitrided plastic mould steel, *Surf. Coat. Technol.*, 334 (2018), 116–123, doi:10.1016/j.surfcoat.2017.11.033
- Y. Qian, C. Ma, D. Niu, J. Xu, M. Li, Influence of alloyed chromium on the atmospheric corrosion resistance of weathering steels, *Corros. Sci.*, 74 (2013), 424–429, doi:10.1016/j.corsci.2013.05.008
- J. H. Hong, S. H. Lee, J. G. Kim, J. B. Yoon, Corrosion behaviour of copper containing low alloy steels in sulphuric acid, *Corros. Sci.*, 54 (2012), 174–182, doi:10.1016/j.corsci.2011.09.012
- Y. Zhou, J. Chen, Y. Xu, Z. Liu, Effects of Cr, Ni and Cu on the corrosion behavior of low carbon microalloying steel in a Cl<sup>-</sup> containing environment, *J. Mat. Sci. Tech.*, 29 (2013) 2, 168–174, doi:10.1016/j.jmst.2012.12.013
- L. Hao, S. Zhang, J. Dong, W. Ke, Atmospheric corrosion resistance of MnCuP weathering steel in simulated environments, *Corros. Sci.*, 53 (2011) 12, 4187–4192, doi:10.1016/j.corsci.2011.08.028
- Y.-S. Choi, J.-J. Shim, J.-G. Kim, Effects of Cr, Cu, Ni and Ca on the corrosion behavior of low carbon steel in synthetic tap water, *J. Alloys Compd.*, 391 (2005) 1, 162–169, doi:10.1016/j.jallcom.2004.07.081
- L. Y. Lan, C. L. Qiu, D. W. Zhao, X. H. Gao, L. X. Du, Analysis of martensite-austenite constituent and its effect on toughness in submerged arc welded joint of low carbon bainitic steel, *J. Mat. S.*, 47 (2012) 11, 4732–4742, doi:10.1007/s10853-012-6346-x
- Z. Zhang, X. C. Wu, N. Li, Y. A. Min, Alloy optimisation of bainitic steel for large plastic mould, *Mater. Sci. Technol.*, 31 (2015) 14, 1706–1714, doi:10.1179/1743284714Y.0000000744
- C. Zhang, K. Yamanaka, H. Bian, A. Chiba, Corrosion-resistant carbide-reinforced martensitic steel by Cu modification, *NPJ Materials Degradation*, 3 (2019) 1, doi:10.1038/s41529-019-0092-3
- J. Guo, S. Yang, C. Shang, Y. Wang, X. He, Influence of carbon content and microstructure on corrosion behaviour of low alloy steels in a Cl<sup>-</sup> containing environment, *Corros. Sci.*, 51 (2009) 2, 242–251, doi:10.1016/j.corsci.2008.10.025
- X. Q. Liu, Z. L. Liu, J. D. Hu, Z. G. Hou, Q. C. Tian, H. Z. Wang, The corrosion behavior of Cu/Cr containing tube pile steel in half-immersion environment, *Anti-Corros. Method. M.*, 63 (2016) 4, 281–288, doi:10.1108/ACMM-10-2014-1441
- M. Yamashita, H. Miyuki, Y. Matsuda, H. Nagano, T. Misawa, The long term growth of the protective rust layer formed on weathering steel by atmospheric corrosion during a quarter of a century, *Corros. Sci.*, 36 (1994) 2, 283–299, doi:10.1016/0010-938X(94)90158-9
- T. Ishikawa, K. Takeuchi, K. Kandori, T. Nakayama, Transformation of  $\gamma$ -FeOOH to  $\alpha$ -FeOOH in acidic solutions containing metal ions, *Colloids Surf. Physicochem. Eng. Aspects*, 266 (2005) 1–3, 155–159, doi:10.1016/j.colsurfa.2005.06.024
- X. Hao, J. Dong, J. Wei, I.-I. N. Etim, W. Ke, Effect of Cu on corrosion behavior of low alloy steel under the simulated bottom plate environment of cargo oil tank, *Corros. Sci.*, 121 (2017), 84–93, doi:10.1016/j.corsci.2017.03.012
- T. Ishu, T. Ujiro, E. Hamada, S. Ishikawa, Y. Kato, A mechanism of improvement in the corrosion resistance of ferritic stainless steels by Cu addition, *Tetsu-to-Hagané / Steel Science Portal*, 97 (2011) 8, 441–449, doi:10.2355/tetsutohagane.97.441